Energy & Environmental Science

Revealing Unprecedented Cathode Interface Behavior in All-Solid-State Batteries with Oxychloride Solid Electrolytes

Journal:	*Energy & Environmental Science*
Manuscript ID	EE-ART-02-2024-000750.R1
Article Type:	Paper
Date Submitted by the Author:	28-Mar-2024
Complete List of Authors:	Zhao, Feipeng; Western University, Department of Mechanical and Materials Engineering Zhang, Shumin; Western University Wang, Shuo; University of Maryland at College Park Andrei, Carmen; McMaster University, Canadian Centre for Electron Microscopy Yuan, Hui; McMaster University, Zhou, Jigang; Canadian Light Source Inc Wang, Jian; Canadian Light Source Inc Zhuo, Zengqing; Lawrence Berkeley National Laboratory, Advanced Light Source Zhong, Yu; Zhejiang University School of Materials Science and Engineering Su, Han; University of Western Ontario Kim, Jung Tae; University of Western Ontario, Yu, Ruizhi; Western University Gao, Yingjie; Western University Guo, Jinghua; Lawrence Berkeley National Laboratory Sham, Tsun-Kong; University of Western Ontario, Chemistry Mo, Yifei; University of Maryland at College Park, Materials Science and Engineering Sun, Xueliang; University of Western Ontario, Mechanical and Materials Engineering

Broader context statement

As the latest generation of solid electrolytes (SEs), lithium metal oxychlorides can deliver ultrahigh ionic conductivity up to 10^{-2} S cm^{-1} that can be comparable to the state-of-the-art sulfide SEs and liquid electrolytes. However, the cathode compatibility between oxychloride SEs and various conventional layered oxide cathode active materials remains ambiguous. Herein, we take the lithium tantalum oxychloride (LTOC) as an example, to investigate its compatibility with three typical CAMs: $LiCoO_2$ (LCO), $LiNi_{0.5}Co_{0.2}Mn_{0.3}O_2$ (NCM523), and $LiNi_{0.83}Co_{0.11}Mn_{0.06}O_2$ (NCM83). Unexpectedly, cobalt-less NCM83 is found to be the most compatible with LTOC SEs, because (i) the Co-poor composition of NCM83 relieve the detrimental Co/Ta interaction, and (ii) the in-situ formed passivation layer eliminates the negative effect of thermodynamic instability between the Ni-rich cathode and LTOC. In spite of this, reducing temperature is verified to significantly improve the cycling durability when using LCO or NCM523. Therefore, coupling the cathode composition and working temperature is proposed as a feasible approach to realize kinetically stabilized cathode/oxychloride interfaces. Our study uncovers an unprecedented cathode interface behavior with oxychloride SEs, which will provide an important guidance in achieving high-energy-density all-solid-state batteries.

Revealing Unprecedented Cathode Interface Behavior in All-Solid-State Batteries with Oxychloride Solid Electrolytes

Feipeng Zhao,[a]‡ Shumin Zhang,[a]‡ Shuo Wang,[c] Carmen M. Andrei,[d] Hui Yuan,[d, e] Jigang Zhou,[f] Jian Wang,[f] Zengqing Zhuo,[g] Yu Zhong,[h] Han Su,[h] Jung Tae Kim,[a] Ruizhi Yu,[a] Yingjie Gao,[a] Jinghua Guo,[g] Tsun-Kong Sham,[i] Yifei Mo,[c] Xueliang Sun[a, b]*

[a] Department of Mechanical and Materials Engineering, Western University, London, ON, N6A 5B9, Canada

[b] Eastern Institute for Advanced Study, Eastern Institute of Technology, Ningbo, Zhejiang 3150200, P.R. China

[c] Department of Materials Science and Engineering, University of Maryland, College Park, MD 20742, USA

[d] Canadian Centre for Electron Microscopy, McMaster University, Hamilton, ON, L8S 4M1, Canada

[e] Department of Materials Science and Engineering, McMaster University, Hamilton, ON, L8S 4L7, Canada

[f] Canadian Light Source Inc., University of Saskatchewan, Saskatoon, SK, S7N 2V3, Canada

[g] Advanced Light Source, Lawrence Berkeley National Laboratory, Berkeley, CA 94720, USA

[h] State Key Laboratory of Silicon Materials, Key Laboratory of Advanced Materials and Applications for Batteries of Zhejiang Province, School of Materials Science & Engineering, Zhejiang University, Hangzhou 310027, China

[i] Department of Chemistry, Western University, London, ON, N6A 5B7, Canada

Corresponding E-mail address: xsun9@uwo.ca

Abstract

All-solid-state lithium batteries (ASSLBs) are highly desirable for their sustainability, enhanced safety, and increased energy densities. The compatibility between cathodes and solid electrolytes (SEs) is critical for ASSLB electrochemical performance. While the conventional $LiCoO_2$ (LCO) cathode shows structural stability, limitations in the energy density and materials cost prompt exploration of Ni-rich, Co-poor cathodes like lithium nickel cobalt manganese oxide (NCM). However, Ni-rich NCM faces challenges with typical solid electrolytes (e.g., sulfides or oxides), hindering high-energy-density ASSLBs. Our study reveals a unique cathode/electrolyte interface behavior with lithium tantalum oxychlorides (LTOC) superionic conductors, favoring Co-less, Ni-rich NCM over LCO. The Ta/Co interaction is identified as a failure mechanism for LTOC/LCO, while a kinetically stabilized interface is achieved with lean-Co cathodes. Beyond the cathode material composition, our study also establishes a correlation between the temperature used for battery testing and both interface reactivity and cell performance. This research provides crucial insights for the innovative design of high-performance ASSLBs based on the promising LTOC oxychloride SEs.

Keywords: all-solid-state lithium batteries, oxychloride solid electrolytes, Co-less cathodes, interface stability

Introduction

All-solid-state lithium batteries (ASSLBs) have gained considerable interest due to their potential to enable high energy density and improved safety.[1-3] Solid electrolytes (SEs) are a critical component of ASSLBs, and significant development of SEs has taken place since the first report of $Li_{10}GeP_2S_{12}$ (LGPS),[4] which exhibited competitive ionic conductivity (> 10^{-2} S cm^{-1}) compared to conventional liquid electrolytes.[5-8] Following LGPS, several sulfide-based SEs have been reported to possess ultrahigh ionic conductivity.[9-11] However, interface instability at both the anode and cathode interface hinders the practical application of sulfide-based ASSLBs.[12-14] Besides pursuing satisfactory ionic conductivities of advanced SSEs for the development of ASSLBs, a considerable amount of research has been devoted to solving those interface challenges in the field of ASSLBs.[8, 15-17]

The desirable cathode interface stability appeals to revisit halide-based SEs, particularly the chloride SEs.[18-21] The intrinsically high anodic stability (> 4.2 V vs. Li/Li^+) of chloride SEs enables high-performance ASSLBs using conventional layered oxide cathode active materials (CAMs).[22] However, the ionic conductivity of chloride SEs has been insufficient (i.e., at the level of 10^{-3} S cm^{-1}),[23, 24] until the report of oxychloride SEs.[25, 26] Among the reported oxychlorides till now,[25-30] Ta-based oxychlorides (Li-Ta-O-Cl or LTOC) exhibit the highest ionic conductivity of 1.24×10^{-2} S cm^{-1} and demonstrates excellent rate capability with layered oxide cathode materials.[25, 26] Nonetheless, with regard to the LTOC oxychloride SE based on the new mixed-anion (Cl and O) chemistry,[28] the understanding on the interface between LTOC and various cathode materials is still very limited. Although the cathode interface between chloride SEs and conventional CAMs is regarded stable, the introduced corner-sharing O in LTOC could influence the interface stability against CAMs. Specifically, all structural O atoms have be verified located at joint sites to generate

"Ta-O-Ta" skeleton in the structure of LTOC,[26] which delivers high-degree-of-freedom and benefits to the Li-ion transport via broadening the energy landscape.[28, 31] Nevertheless, the "flexibility" of corner-sharing O environment brings about the possibility that decomposing the LTOC to constitute different cathode electrolyte interfaces (CEIs) with various CAMs.

In this work, the interface stability between LTOC and conventional layered oxide CAMs, namely $LiCoO_2$ (LCO), $LiNi_{0.5}Co_{0.2}Mn_{0.3}O_2$ (NCM523), and $LiNi_{0.83}Co_{0.11}Mn_{0.06}O_2$ (NCM83), is investigated. These specific CAMs are chosen because they share a similarly layered crystal structure, but with different contents of transition metal elements (Ni, Co, Mn). The morphologies of each kind of CAMs are suggested in **Figure S1** (ESI†). Similar particle size and polycrystalline feature exclude size and morphology effects on the electrochemical performance.[32, 33] As displayed in the **Scheme 1**, it is unexpected to find that Co is more kinetically active than other two transition metals (Ni and Mn) when cycling against the LTOC SE, although the chemical reactivity (thermodynamically) between LTOC and Ni-containing CAMs are considered relatively higher than that of the LTOC/LCO interface. Different from the active Co/Ta interaction at the LTOC/LCO interface, isolated interphase passivation with diacritical reaction boundaries are observed at the LTOC/NCM interfaces. The self-terminating interface reaction of the latter makes the LTOC SE prefers Ni-rich (Co-less) CAMs to achieve high electrochemical performance at room temperature (RT). In addition, the strategy of reducing the working temperature is effective to suppress the kinetic diffusion of Co at the LTOC/LCO interface, thus improving the cycling stability of LCO solid cells. The low-temperature (LT) control is also verified to decrease the thermodynamic reactivity of LTOC/NCM interfaces, providing us new insights into the design of high-performance ASSLBs.

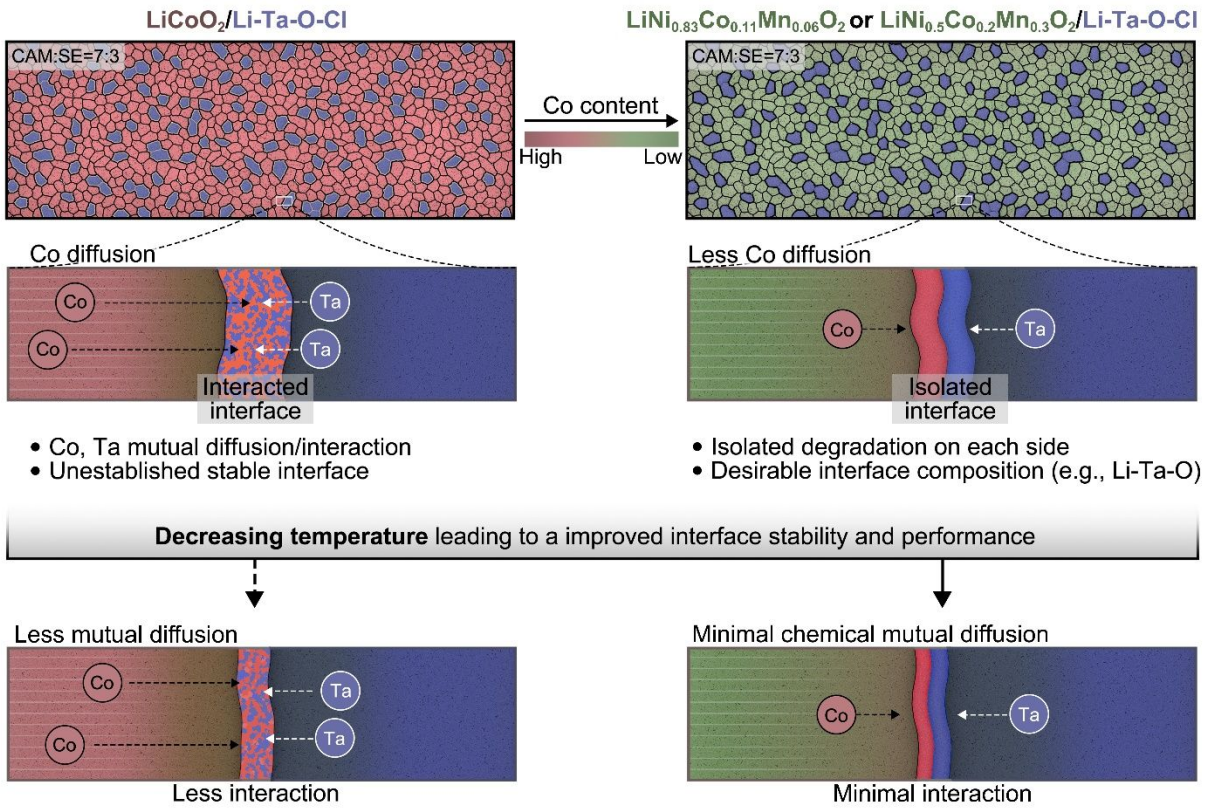

Scheme 1. Illustration on the temperature-dependent interface formation between the Li-Ta-O-Cl (LTOC) SE and conventional cathode materials with different Co contents.

Results and Discussion

Performance of LTOC-based ASSLBs using LCO, NCM523, and NCM83

Ni-rich cathode active materials (CAMs) used in lithium-ion batteries often face structural instability during (de)intercalation when liquid electrolytes are used.[34] However, in an all-solid-state configuration using the LTOC SE, the Ni-rich NCM83 cell exhibited superior stability compared to the other two selected CAMs, namely LCO and NCM523, as depicted in **Figure 1a**. When cycled at RT and 0.2 C, the NCM83 solid cell showed a high capacity retention of 96% (calculation relative to the first-cycle capacity, the same after here) after 50 cycles, which was in sharp contrast to the NCM523 (85%) and LCO (78%) cells. The cycling stability for both the LCO

and NCM523 solid cells could be improved significantly by simply lowering the cell test temperature (**Figure 1b**). When tested at 0.2 C and -10 ℃, the capacity retentions maintained as high as 86% and 95% after 200 cycles for the LCO and NCM523 solid cells, respectively. Furthermore, the benefit of lowering operating temperature for the enhanced cycling stability was also verified at current densities of 0.5 C and 1 C (**Figure S2**, ESI†). The improved cycling performance (particularly for the LCO and NCM523 solid cells) through lowering the working temperature is summarized and depicted in **Figure 1c**. At other different current densities, ranging from 0.05 C to 1 C, both LCO (**Figure 1d-e**) and NCM523 (**Figure 1f-g**) solid cells also demonstrated improved electrochemical reversibility. In contrast, the improvement degree for the NCM83 cell by lowering the operating temperature is subtle (**Figure 1h-i**), even though the excellent long-term cycling stability (85% retention after 3000 cycles) was achieved at -10℃ (**Figure S3**, ESI†). However, it should be noted that the reversible capacity of all solid cells at -10 ℃ decreased at each specific current density due to sluggish electrochemical reaction kinetics of the electrode at low temperatures,[9, 35] which resulted in increased polarization during charging and discharging, as indicated in **Figure S4** (ESI†).

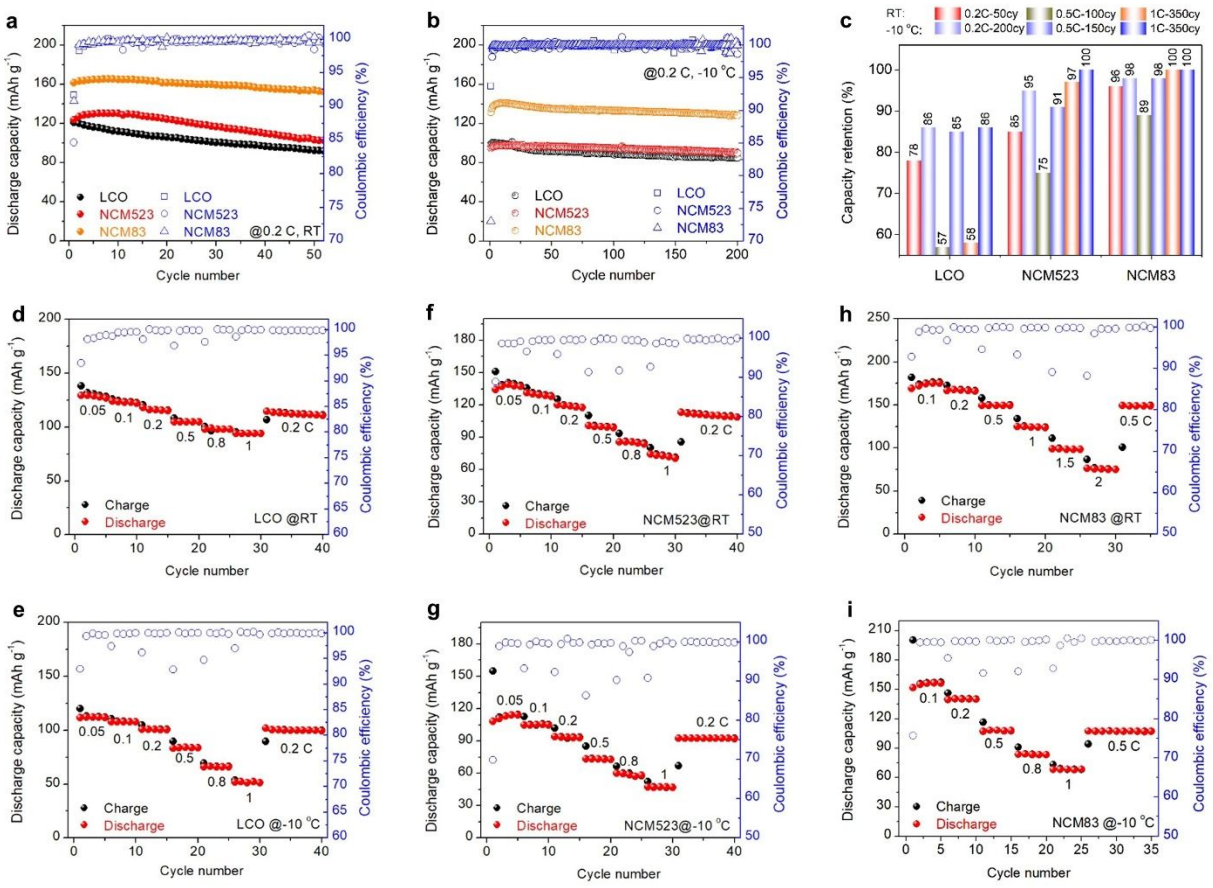

Figure 1. Electrochemical performance of ASSLBs using the LTOC SE coupling with different CAMs. (a) Cycling stability of using NCM83, NCM523, and LCO at a low current density of 0.2 C (RT). (b) Cycling stability of using NCM83, NCM523, and LCO at a low current density of 0.2 C and a low temperature of -10 ℃. (c) Comparison of the capacity retention after cycling in the solid cells at various current densities (0.2 C, 0.5 C, and 1 C) and temperatures (RT and -10 ℃). (d, e) Rate capabilities of the LCO cells measured at RT and -10 ℃, respectively. (f, g) Rate capabilities of the NCM523 cells measured at RT and -10 ℃, respectively. (h, i) Rate capabilities of the NCM83 cells measured at RT and -10 ℃, respectively. Note: the loading mass of CAMs in various solid cells was around 5 mg.

Temperature-dependent electrochemical behaviors

As the composition of NCM523 is moderate compared with the Co-rich LCO or Ni-rich NCM83, we firstly used NCM523 as a model CAM to examine the temperature-dependent electrochemical behavior when cycling against the LTOC SE. Variable-rate cyclic voltammetry (CV) measurements were carried out for the NCM523 solid cells at three different temperatures (RT, -10 ℃, and 60 ℃), as depicted in **Figure 2a-c**. Both anodic and catholic peak currents were increased along with elevated scanning rates at RT or -10 ℃, but became abnormal at 60 ℃ when using relatively high scanning rates (over 0.15 mV s^{-1}). Linear fitting of the peak currents for the RT and -10 ℃ (**Figure 2d** and **e**) derived slopes between 0.5 and 1. It is reported that the slope of 0.5 indicates an ideal situation where a (de)intercalation reaction happens to the working electrode using layered oxide CAMs[36]. Deviated value towards 1 implies the uptake of capacity is contributed partially by Li-ion diffusion process, which is generally dominated by the formation of CEIs.[36] At -10 ºC, the anodic slope value (0.56) was much closer to 0.5 than that at RT (0.73), suggesting that the CEI formed at -10 ℃ showed much less influence than that at RT on the de-intercalation reaction of NCM523 CAMs. This was also verified by collecting the electrochemical impedance spectroscopy (EIS) plots for the NCM523 solid cells cycled (RT and -10 ℃) after different cycles (**Figure S5**, ESI†). Increasing the temperature to 60 ℃ deteriorated the CEI stability, because the linear fitting was even not adaptable due to the diverging data points as displayed in **Figure 2f**. The similarly abnormal redox reaction during the CV measurements occurred to the LCO cell operating at 60 ℃, but was greatly eliminated in the NCM83 counterpart (**Figures S6** and **S7**, ESI†), indicating the Co content in the CAMs could be as one of the important factors to determine the CEI stability against the LTOC SE. Even so, increasing temperature was demonstrated to deteriorate the cycling performance of LTOC-based solid cells using these three kinds of CAMs (**Figure S8**, ESI†).

Constant current intermittent titration (GITT) measurements were further conducted on the NCM523 solid cells, as shown in **Figure S9** (ESI†). The GITT measurement for the solid cell has been reported that not only detect the Li-ion relaxation, but also indicate the influence of interface degradation.[37] Derived from the GITT measurements at various temperatures, Li-ion diffusivity in the NCM523 electrode were recorded against the relaxation potential as described in **Figure 2g-i**. In the first charging (delithiation) process, high temperature (HT, i.e., 60 ℃) brought about faster Li-ion transport in the electrode, showing a higher diffusivity mostly above 10^{-10} cm^2 s^{-1}. Meanwhile, the growth of CEI at HT was the most prominent (comparing to RT or LT situation). The generated CEI even hindered Li-ion diffusion in the subsequent discharging (lithiation) process, as the Li-ion diffusivity at HT was lower than that in RT during discharging. Additionally, it was shown that in the effective (de)interclation regions, the LT case presented the highest degree-of-overlap in the diffusivity values during charging and discharging, while the HT case was the worst. These phenomena implied that the LT condition benefited to generate stabilized CEI and achieved highly reversible (de)interclation reactions. Similar results were also reported by Janek et al. for the sulfide-based ASSLBs,[38] where LT was helpful for stabilizing the interface impedance between LGPS and $LiNi_{0.6}Co_{0.2}Mn_{0.2}O_2$ (NCM622) CAMs, because the interfacial reaction rate constant (k) was exponentially correlated to the temperature.

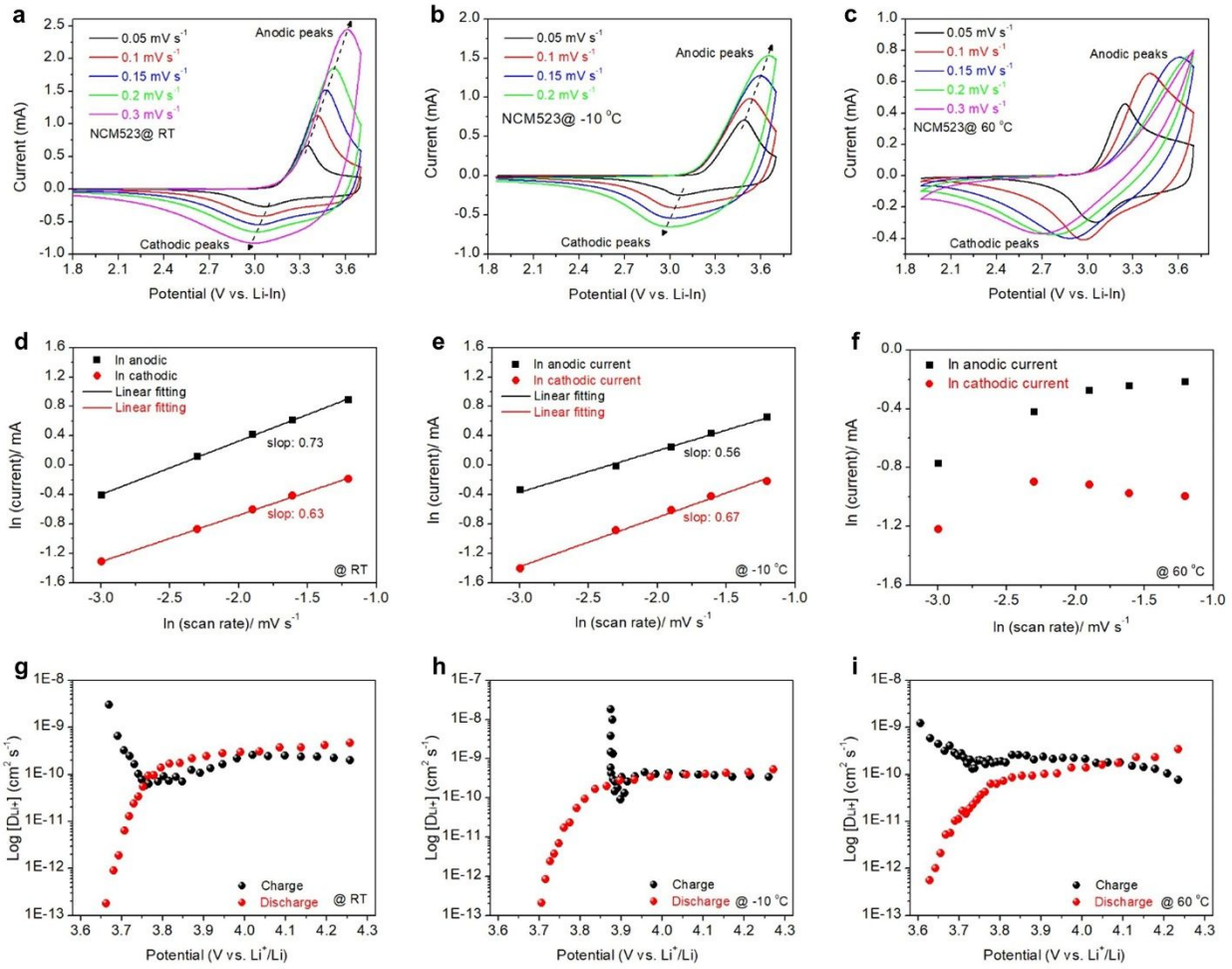

Figure 2. Temperature-dependent electrochemical behaviors in the NCM523 cells. (a-c) CV curves of the NCM523 cells measured at various scan rates at RT, -10 ℃ (LT), and 60 ℃ (HT), respectively. (d-f) The linear fittings for the scanning rate-dependent cathodic and anodic peak currents from (a-c). (g-i) Constant current intermittent titration (GITT) measurements on the NCM523 cells performed at 0.1 C under RT, -10 ℃, and 60 ℃, respectively.

Characterizations on the LTOC/CAMs interfaces

As shown above, the CEI stability between LTOC and CAMs is temperature-dependent, which plays a crucial role to influence the electrochemical behavior and determine the LTOC-based solid cell performance. To elucidate the interface composition of LTOC/CAMs and the intrinsic reason

of the discrepant interface stability using different CAMs, we combined various physicochemical characterizations to study LTOC/CAM interfaces. First, thermodynamic calculations provided us the phase equilibria between LTOC and the three CAMs. As shown in **Table 1**, all three CAMs (NCM83, NCM523, LCO) are not thermodynamically stable with the LTOC SE, due to the favorable interface reaction.[39, 40] In addition to thermodynamic equilibrium, as many theoretical and experimental reports have verified, the inclusion of considering kinetic factors (e.g., interphase passivation layer) at the interface is critical in determining the formation of CEI and interface stability[14, 41]. It has been suggested that the detrimental element mutual diffusion[42] was only observed for the interface of LTOC/LCO leading to the formation of Ta_2CoO_6. Similarly, the Co-involved mutual diffusion was observed at the cathode interface in SSBs based on either sulfide or oxide SSEs.[42, 43] For example, inter-diffusion of Co, La, and Zr cations was reported at the interface between LCO and $Li_7La_3Zr_2O_{12}$ SE with the formation of La_2CoO_4,[43] which was even believed as the starting point of the interface degradation.[44] By contrast, the NCM CAMs with lower Co contents (i.e., NCM523 and NCM83) avoided the formation of the interplayed products at the interface. Instead, the ion-conducting $LiTa_3O_8$ was predicted as one of the reaction products at the interface of LTOC/NCM, which could contribute as a favorable passivation layer of CEIs for Li-ion exchange.[39, 45] The interphase discrepancy was also verified by the in-situ EIS plots recorded in the first charge/discharge process of cycling LCO and NCM83 CAMs, as displayed in **Figure S10** (ESI†). LTOC/LCO interface impedance was continuously increased, while the LTOC/NCM83 showed a much less interface impedance after the first charge/discharge.

Table 1. Thermodynamic calculation of the interphase composition between the LTOC SE and various cathode materials.

Cathode	Composition	x_{SE}	Phase equilibria at x_m
LCO	$LiCoO_2$	0.34	Ta_2CoO_6, LiCl, $LiCo_2O_4$, Co_3O_4
	$Li_{0.5}CoO_2$	0.36	Ta_2CoO_6, LiCl, $CoCl_2$, CoO_2
NCM523	$LiNi_{0.5}Co_{0.2}Mn_{0.3}O_2$	0.38	LiCl, $LiTa_3O_8$, $Mn(Ni_3O_4)_2$, $MnNiO_3$, CoO_2
	$Li_{0.5}Ni_{0.5}Co_{0.2}Mn_{0.3}O_2$	0.42	LiCl, Ta_2O_5, O_2, $NiCl_2$, CoO_2, $MnNiO_3$
	$Li_{0.2}Ni_{0.5}Co_{0.2}Mn_{0.3}O_2$	0.64	LiCl, Ta_2O_5, Cl_2, $NiCl_2$, CoO_2, MnO_2
NCM83	$LiNi_{0.83}Co_{0.11}Mn_{0.06}O_2$	0.38	LiCl, $LiTa_3O_8$, O_2, NiO, $Mn(Ni_3O_4)_2$, CoO_2
	$Li_{0.5}Ni_{0.83}Co_{0.11}Mn_{0.06}O_2$	0.62	LiCl, Ta_2O_5, O_2, $NiCl_2$, CoO_2, $MnNiO_3$
	$Li_{0.2}Ni_{0.83}Co_{0.11}Mn_{0.06}O_2$	0.61	LiCl, Ta_2O_5, O_2, $NiCl_2$, CoO_2, $MnNiO_3$

Then, the morphologies and chemical distribution details of LTOC/CAM interfaces (after cycling at RT) were obtained experimentally by conducting electron microscopy (EM) characterizations. The use of nanosized LTOC SEs effectively enveloped the CAM particles, thus ensuring adequate Li-ion transport pathways, as demonstrated in **Figures S11** and **S12** (ESI†). This eliminates any possibility of interface issues arising from a lack of effective physical contact in our analyses. The high-resolution transmission electron microscopy (HRTEM) image of the LTOC/LCO interface revealed that LiCl compounds were embedded in the amorphous matrix (**Figure 3a**). The recognition of the LiCl component agreed with the predicted interfacial products above. In addition, Cl was considered rich at the LTOC/LCO interface according to the electron energy loss spectroscopy (EELS) element mapping (**Figure 3b**), which affirmed that the interfacial reaction between LTOC and LCO is significant at RT. More interestingly, Co was found diffused deeply across the interface and headed toward the bulk area of LTOC, which was also reflected by the

evolution of Co L-edge EELS spectra across the LTOC/LCO interface, as indicated in **Figure 3c**. The gradual low-energy shift of the Co L-edge suggested that the oxidation state of Co (III) was reduced, which emerged at the interface and extended to the distance over 100 nm. In sharp contrast, the interface of LTOC/NCM83 showed distinct reaction boundaries as demonstrated in the EELS element mapping (**Figure 3d**). Furthermore, as displayed in **Figure 3e**, a series of EELS spectra across the LTOC/NCM83 interface indicated that Co (III) was kept unchanged, but Ni from the NCM83 was chemically reduced at the interface. The estimated thickness of the LTOC/NCM83 interface was around 45 nm via measuring the penetration depth of reduced-Ni species. The transition metal penetration length was significantly lower than that at the LTOC/LCO interface, proving the LTOC/NCM83 interface was more passivated kinetically. In addition, the element diffusion became serious at an elevated temperature of 60 ℃. As shown in **Figure S13** (ESI†), even for the moderate composition of NCM523, the interphase layer could reach ~150 nm according to the EDS line scan for the FIB-cut cathode sample. Accompanying the chemical reduction of Ni, Ta species (e.g., Ta is possibly in the form of $LiTa_3O_8$ or Ta_2O_5 according to the thermodynamic calculations) showing higher oxidization state (comparing to Ta in LTOC) could be generated at the LTOC/NCM83 interface. The chemically oxidized (high-energy shift) Ta species were also experimentally confirmed by conducting X-ray photoelectron spectroscopy (XPS) analyses for the cycled LTOC/NCM83 composite as suggested in **Figure S14** (ESI†). In contrast to the distinct chemical evolution of transition metal elements (i.e., Co, Ni, and Ta), O was considered stable at the LTOC/CAM interfaces as displayed in the X-ray absorption spectroscopy (XAS) of O K-edge (**Figure S15**, ESI†).

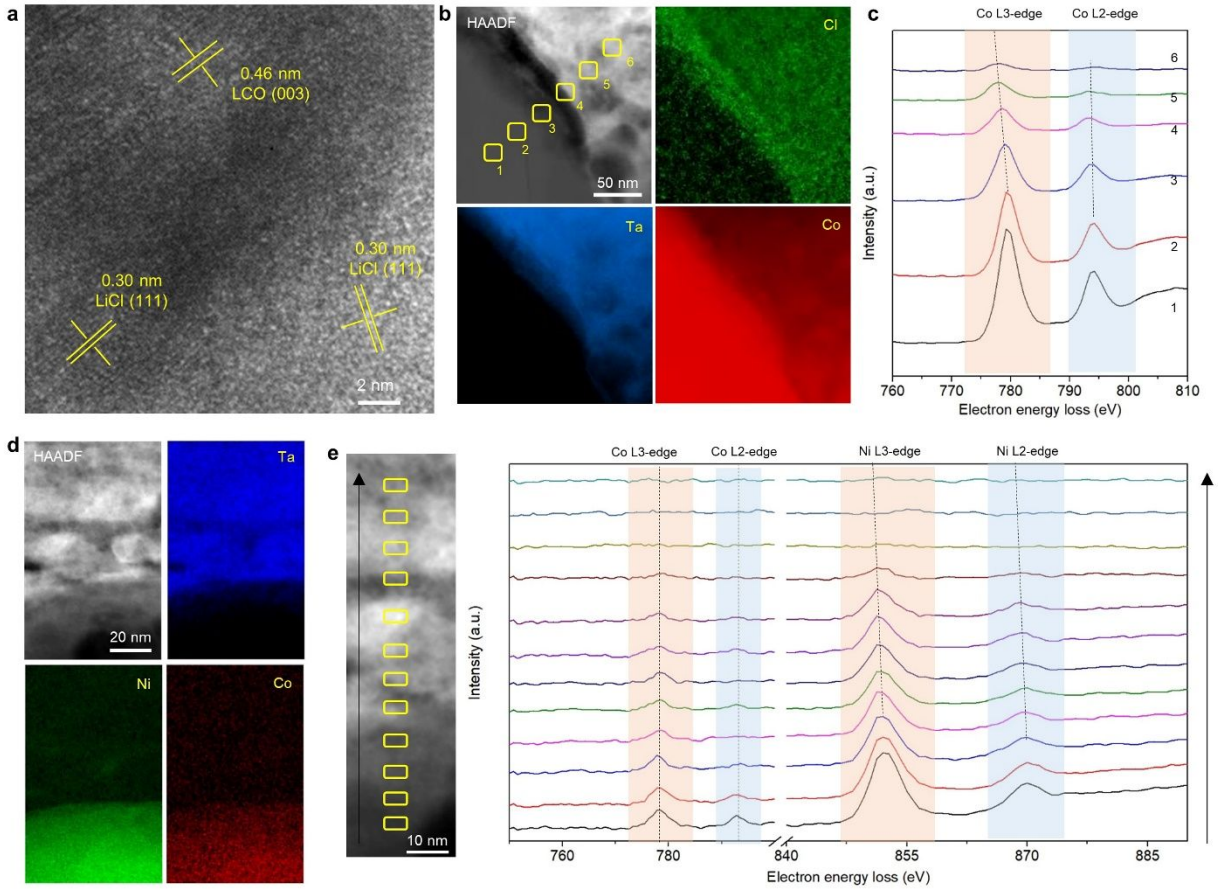

Figure 3. TEM-EELS characterizations on CAM/LTOC interfaces cycled at RT. (a) HRTEM image of the LCO/LTOC interface. (b) High-angle annular dark-field (HAADF) image and EELS element mapping at the LCO/LTOC interface. (c) EELS spectra of the Co L-edge in the marked positions of the HAADF image. (d) HAADF image and EELS element mapping at the NCM83/LTOC interface. (e) HAADF image of the NCM83/LTOC interface and EELS spectra extracted in selected area across the interface. Note: the interface samples were prepared by plasma focused ion beam (PFIB) instrument; the EELS scanning step was set as 1 nm.

We further employed scanning transmission X-ray microscopy (STXM) to obtain chemical information of specific CAM particles after cycling against the LTOC SE under various temperatures. One advantage of using STXM compared with only using TEM-EELS is that it can

provide higher energy resolution in analyzing the chemistry nature of interfaces.[46, 47] As shown in **Figure 4a**, the yellow-circled particles were identified as LCO, which was connected to the surrounding LTOC particles. The details about locating CAMs particles in the cathode composites were described in **Figure S16** (ESI†). It was found from the series spectra of Co L-edge (**Figure 4b**) that both reduced and oxidized Co (III) species occurred on the cycled LCO particles at RT and HT, while the shape feature of Co L-edge remained unchanged at LT. The reduced Co (III) might exist in the form of Ta_2CoO_6, Co_3O_4, or $CoCl_2$, while the oxidized Co could be from $LiCo_2O_4$ or CoO_2 (based on the thermodynamic calculations). The suppressed side reaction upon decreasing the test temperature for the LCO solid cells was corresponding to enhanced cycling stability at LT as we discussed in the electrochemistry part. By contrast, the cycled NCM523 and NCM83 particles (RT) identified by the STXM (**Figure S17**, ESI†) only showed Co-oxidized components as indicated in **Figure 4c** and **Figure 4d**, respectively. Thus, echoing to the TEM-EELS results, the chemical activity between Co-rich LCO and LTOC SEs was experimentally verified, while the LT control demonstrated a feasible approach to reduce the reactivity. Besides, using Co-less NCM CAMs (i.e., NCM523 or NCM83) was confirmed to alleviate the interface reactivity by forming satisfactory interfacial passivation layers.

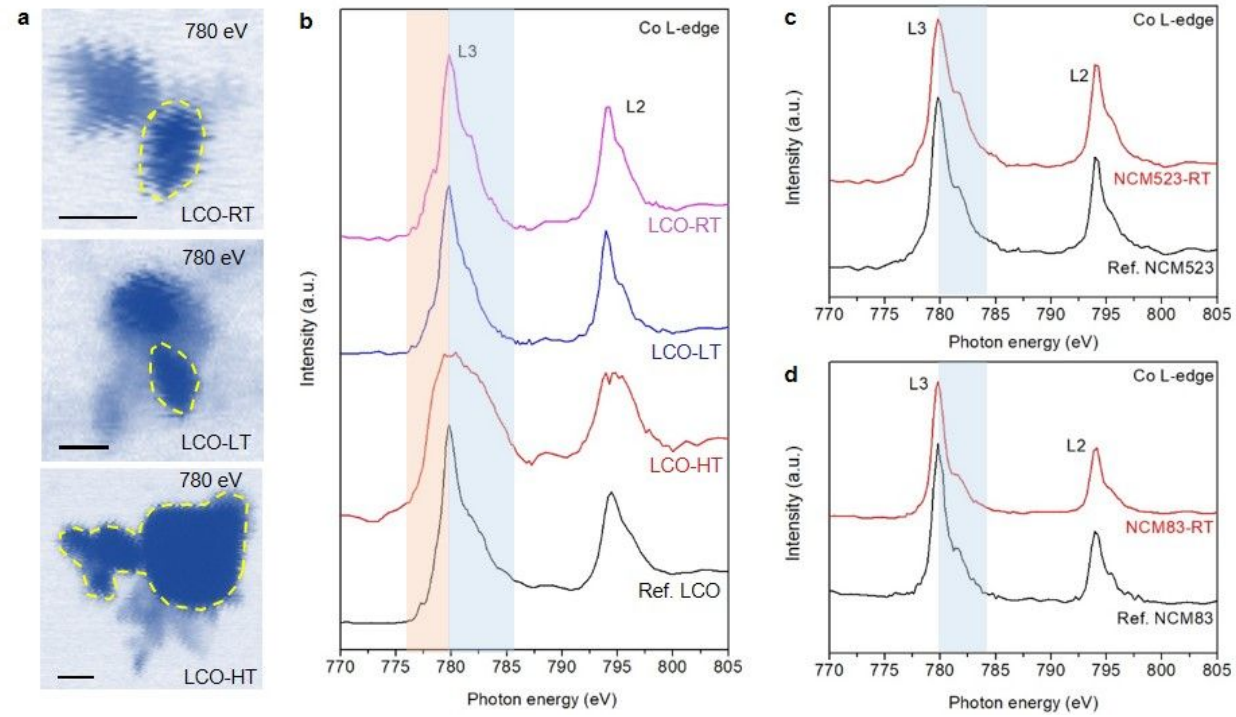

Figure 4. STXM characterizations on the LTOC/CAM interfaces. (a) LCO particles (circled in yellow) located by the STXM at an absorption energy of Co (780 eV). The LCO CAMs were obtained after cycling for 20 cycles at 0.1 C and under various temperature. RT: 25 ℃; LT: -10 ℃; HT: 60 ℃. Scale bar: 500 nm. (b) The XAS spectra of Co L-edge of the identified LCO particles in (a). (c and d) The XAS spectra of Co L-edge of the NCM523 and NCM83 particles after cycling (20 cycles, 0.1 C and RT), respectively.

Conclusions

In this work, we investigated the temperature-dependent electrochemical performance of LTOC-based ASSLBs using three CAMs with varying transition metal compositions: LCO, NCM523, and NCM83. We unexpectedly found that at room temperature, LTOC showed better cycling stability when paired with Ni-rich NCM83 CAMs. However, reducing the temperature significantly improved the cycling durability of LCO and NCM523 CAMs. These results were

attributed to the interface stabilities between LTOC and CAMs based on a comprehensive consideration of both thermodynamic and kinetic factors. Our experiments confirmed that the active LTOC/LCO interface is created by kinetically active Co species diffusing to the Ta-based oxychloride. However, this negative kinetic effect is alleviated by reducing the working temperature. On the other hand, the LTOC/NCM83 interface is thermodynamically unstable, but is self-evolutionary through the formation of passivated interphase, which prevents further decomposition. In the case of NCM523, there is still an off-balance between the negative kinetic effect and the positive thermodynamic effect. As a result, the electrochemical performance at room temperature is moderate, but there is some improvement in cycling stability when the temperature is reduced. Our study provides insight into how the composition of cathode materials and the working temperature of oxychloride-based ASSLBs can affect the cathode interface stability.

Author Contributions

F.Z. and X.S. conceived the project. F.Z. and S.Z. performed the electrolyte synthesis and electrochemical performance characterizations. S.W. performed the computational simulations under the supervision of Y.M. J.W., J.Z., and Y.G. helped in the STXM measurements and analyses. C.A. and H.Y. helped with EM measurements. J.F. and T.S. suggested on the synchrotron-based data analysis. Z.Z and J.G. helped with the O K-edge measurements and analyses. Y.Z., H.S., J.T.K., and R.Y. advised the electrochemical characterizations. F.Z. and S.Z. formally analyzed all data and wrote the manuscript. X.S. supervised the project. All the authors participated in the reviewing and editing of the manuscript.

Conflicts of interest

There are no conflicts to declare.

Acknowledgments

Authors thank the support from the Natural Sciences and Engineering Research Council of Canada (NSERC), the Canada Research Chair Program (CRC), the Canada Foundation for Innovation (CFI), and Western University. PFIB and TEM work was carried out at the Canadian Centre for Electron Microscopy (CCEM), a national facility supported by NSERC and McMaster University. The authors acknowledge Sabaa Rashid for her kind help with FIB-SEM characterizations. The synchrotron related characterizations was completed at the Canadian Light Source (CLS), which is supported by the CFI, the NSERC, the National Research Council (NRC), the Canadian Institutes of Health Research (CIHR), the Government of Saskatchewan, and the University of Saskatchewan. Soft XAS O-K data were performed at BL7.3.1 of Advanced Light Source (ALS), a U.S. Department of Energy Office of Science User Facility, under DOE contract no. DE-AC02-05CH11231. Y.M. acknowledges the funding support from National Science Foundation under award number 1940166, and the computational facilities from the University of Maryland supercomputing resources.

Footnotes

† Electronic supplementary information (ESI) available. See DOI: 10.1039/x0xx00000x

‡ These authors contributed equally to this work.

References

1. J. Janek and W. G. Zeier, *Nat. Energy*, 2023, **8**, 230–240.
2. Q. Zhao, S. Stalin, C.-Z. Zhao and L. A. Archer, *Nat. Rev. Mater.*, 2020, **5**, 229-252.
3. Y. S. Meng, V. Srinivasan and K. Xu, *Science*, 2022, **378**, eabq3750.
4. N. Kamaya, K. Homma, Y. Yamakawa, M. Hirayama, R. Kanno, M. Yonemura, T. Kamiyama, Y. Kato, S. Hama, K. Kawamoto and A. Mitsui, *Nat. Mater.*, 2011, **10**, 682-686.
5. J. W. Liang, X. N. Li, K. R. Adair and X. L. Sun, *Acc. Chem. Res.*, 2021, **54**, 1023-1033.

6. Z. Zhang, Y. Shao, B. Lotsch, Y.-S. Hu, H. Li, J. Janek, L. F. Nazar, C.-W. Nan, J. Maier, M. Armand and L. Chen, *Energy Environ. Sci.*, 2018, **11**, 1945-1976.
7. A. Manthiram, X. Yu and S. Wang, *Nat. Rev. Mater.*, 2017, **2**, 16103.
8. W. Zhao, J. Yi, P. He and H. Zhou, *Electrochem. Energy Rev.*, 2019, **2**, 574-605.
9. Y. Kato, S. Hori, T. Saito, K. Suzuki, M. Hirayama, A. Mitsui, M. Yonemura, H. Iba and R. Kanno, *Nat. Energy*, 2016, **1**, 16030.
10. L. D. Zhou, A. Assoud, Q. Zhang, X. H. Wu and L. F. Nazar, *J. Am. Chem. Soc.*, 2019, **141**, 19002-19013.
11. Y. Seino, T. Ota, K. Takada, A. Hayashi and M. Tatsumisago, *Energy Environ. Sci.*, 2014, **7**, 627-631.
12. Y. Xiao, Y. Wang, S.-H. Bo, J. C. Kim, L. J. Miara and G. Ceder, *Nat. Rev. Mater.*, 2019, **5**, 105-126.
13. R. Chen, Q. Li, X. Yu, L. Chen and H. Li, *Chem. Rev.*, 2019, **120**, 6820–6877.
14. F. Zhao, S. Zhang, Y. Li and X. Sun, *Small Struct.*, 2022, **3**, 2100146.
15. A. M. Nolan, Y. Zhu, X. He, Q. Bai and Y. Mo, *Joule*, 2018, **2**, 2016-2046.
16. A. Banerjee, X. F. Wang, C. C. Fang, E. A. Wu and Y. S. Meng, *Chem. Rev.*, 2020, **120**, 6878-6933.
17. D. H. S. Tan, A. Banerjee, Z. Chen and Y. S. Meng, *Nat. Nanotechnol.*, 2021, **16**, 479-479.
18. X. N. Li, J. W. Liang, X. F. Yang, K. R. Adair, C. H. Wang, F. P. Zhao and X. L. Sun, *Energy Environ. Sci.*, 2020, **13**, 1429-1461.
19. T. Asano, A. Sakai, S. Ouchi, M. Sakaida, A. Miyazaki and S. Hasegawa, *Adv. Mater.*, 2018, **30**, 1803075.
20. L. Zhou, T.-T. Zuo, C. Y. Kwok, S. Y. Kim, A. Assoud, Q. Zhang, J. Janek and L. F. Nazar, *Nat. Energy*, 2022, **7**, 83–93.
21. K. Tuo, C. W. Sun and S. Q. Liu, *Electrochem. Energy Rev.*, 2023, **6**, 17.
22. S. Wang, Q. Bai, A. M. Nolan, Y. S. Liu, S. Gong, Q. Sun and Y. F. Mo, *Angew. Chem. Int. Ed.*, 2019, **58**, 8039-8043.
23. C. Wang, J. Liang, J. T. Kim and X. Sun, *Sci. Adv.*, 2022, **8**, eadc9516.
24. J. W. Liang, X. N. Li, S. Wang, K. R. Adair, W. H. Li, Y. Zhao, C. H. Wang, Y. F. Hu, L. Zhang, S. Q. Zhao, S. G. Lu, H. Huang, R. Y. Li, Y. F. Mo and X. L. Sun, *J. Am. Chem. Soc.*, 2020, **142**, 7012-7022.
25. Y. Ishiguro, K. Ueno, S. Nishimura, G. Iida and Y. Igarashib, *Chem. Lett.*, 2023, **52**, 237-241.
26. Y. Tanaka, K. Ueno, K. Mizuno, K. Takeuchi, T. Asano and A. Sakai, *Angew. Chem. Int. Ed.*, 2023, **62**, e202217581.
27. K. Wang, Q. Y. Ren, Z. Q. Gu, C. M. Duan, J. Z. Wang, F. Zhu, Y. Y. Fu, J. P. Hao, J. F. Zhu, L. H. He, C. W. Wang, Y. Y. Lu, J. Ma and C. Ma, *Nat. Commun.*, 2021, **12**, 4410.
28. S. Zhang, F. Zhao, J. Chen, J. Fu, J. Luo, S. H. Alahakoon, L.-Y. Chang, R. Feng, M. Shakouri, J. Liang, Y. Zhao, X. Li, L. He, Y. Huang, T.-K. Sham and X. Sun, *Nat. Commun.*, 2023, **14**, 3780.
29. B. Li, Y. Li, H.-S. Zhang, T.-T. Wu, S. Guo and A.-M. Cao, *Sci. China Mater.*, 2023, **66**, 3123–3128.
30. T. Dai, S. Y. Wu, Y. X. Lu, Y. Yang, Y. Liu, C. Chang, X. H. Rong, R. J. Xiao, J. M. Zhao, Y. H. Liu, W. H. Wang, L. Q. Chen and Y. S. Hu, *Nat. Energy*, 2023, **8**, 1221–1228.

31. Z. Z. Zhang and L. F. Nazar, *Nat. Rev. Mater.*, 2022, **7**, 389-405.
32. Y. Han, S. H. Jung, H. Kwak, S. Jun, H. H. Kwak, J. H. Lee, S. T. Hong and Y. S. Jung, *Adv. Energy Mater.*, 2021, **11**, 2100126.
33. X. S. Liu, B. Z. Zheng, J. Zhao, W. M. Zhao, Z. T. Liang, Y. Su, C. P. Xie, K. Zhou, Y. X. Xiang, J. P. Zhu, H. C. Wang, G. M. Zhong, Z. L. Gong, J. Y. Huang and Y. Yang, *Adv. Energy Mater.*, 2021, **11**, 2003583.
34. H. H. Ryu, K. J. Park, C. S. Yoon and Y. K. Sun, *Chem. Mater.*, 2018, **30**, 1155-1163.
35. N. Zhang, T. Deng, S. Zhang, C. Wang, L. Chen, C. Wang and X. Fan, *Adv. Mater.*, 2021, **34**, 2107899.
36. H. Lindstrom, S. Sodergren, A. Solbrand, H. Rensmo, J. Hjelm, A. Hagfeldt and S. E. Lindquist, *J. Phys. Chem. B*, 1997, **101**, 7717-7722.
37. R. Ruess, S. Schweidler, H. Hemmelmann, G. Conforto, A. Bielefeld, D. A. Weber, J. Sann, M. T. Elm and J. Janek, *J. Electrochem. Soc.*, 2020, **167**, 100532.
38. T. T. Zuo, R. Ruess, R. J. Pan, F. Walther, M. Rohnke, S. Hori, R. Kanno, D. Schroder and J. Janek, *Nat. Commun.*, 2021, **12**, 6669.
39. Y. H. Xiao, L. J. Miara, Y. Wang and G. Ceder, *Joule*, 2019, **3**, 1252-1275.
40. A. M. Nolan, Y. S. Liu and Y. F. Mo, *ACS Energy Lett.*, 2019, **4**, 2444-2451.
41. Y. Zhu, X. He and Y. Mo, *ACS Appl. Mater. Interfaces*, 2015, **7**, 23685-23693.
42. A. Sakuda, A. Hayashi and M. Tatsumisago, *Chem. Mater.*, 2010, **22**, 949-956.
43. K. H. Kim, Y. Iriyama, K. Yamamoto, S. Kumazaki, T. Asaka, K. Tanabe, C. A. J. Fisher, T. Hirayama, R. Murugan and Z. Ogumi, *J. Power Sources*, 2011, **196**, 764-767.
44. M. M. U. Din, L. Ladenstein, J. Ring, D. Knez, S. Smetaczek, M. Kubicek, M. Sadeqi-Moqadam, S. Ganschow, E. Salagre, E. G. Michel, S. Lode, G. Kothleitner, I. Dugulan, J. G. Smith, A. Limbeck, J. Fleig, D. J. Siegel, G. J. Redhammer and D. Rettenwander, *Adv. Funct. Mater.*, 2023, **33**, 2303680.
45. Y. Z. Zhu, X. F. He and Y. F. Mo, *J. Mater. Chem. A*, 2016, **4**, 3253-3266.
46. W. H. Li, Z. Q. Wang, F. P. Zhao, M. S. Li, X. J. Gao, Y. Zhao, J. Wang, J. G. Zhou, Y. F. Hu, Q. F. Xiao, X. Y. Cui, M. J. Eslamibidgoli, M. H. Eikerling, R. Y. Li, F. Brandys, R. Divigalpitiya, T. K. Sham and X. L. Sun, *Chem. Mater.*, 2020, **32**, 1272-1280.
47. A. E. Goode, A. E. Porter, M. P. Ryan and D. W. McComb, *Nanoscale*, 2015, **7**, 1534-1548.